CFD simulation and experimental measurement of nickel solids concentration distribution in a stirred tank

by A. Ochieng*, M.S. Onyango†, and K.H. Kiriamiti‡

Synopsis

Solids suspension influences the quality of mixing and energy requirement in a solid-liquid system, both of which determine the efficiency of industrial processes such as nickel precipitation. Nickel solids concentration distribution in a stirred tank was investigated using computational fluid dynamics (CFD) and experimental methods. The concentration distribution of the nickel solids was compared with that of sand and glass. The laser Doppler velocimetry (LDV) method was used to measure the velocity field for the liquid-only system and an optical technique was employed to determine the axial solids concentration distribution. Regions of inhomogeneity in the tank were identified. It was found that, for a given solids loading, the solids concentration distribution depended on both particle size and particle size distribution. High solids loadings were investigated and a difference in the concentration distribution pattern was obtained with nickel, flint glass and sand particles. The CFD simulation results highlighted problems that could be associated with some conventional experimental methods of determining solids concentration distribution in a stirred tank.

Keywords: nickel; CFD; simulation; mixing; solids suspension.

Introduction

In a multiphase system, hydrodynamic characteristics influence phase mixing and mass transfer, and these affect conversion in a reactor. Detailed information on the effects of the hydrodynamics on the performance of an agitated system with high density particles like nickel is still required for the design and operation of hydrometallurgical systems. There is a need to identify and quantify the operating hydrodynamic parameters that influence the quality of mixing, and this can be done by both experimental and simulation methods. Reactions that take place in multiphase systems include nickel precipitation. Nickel is a high density solid and its suspension in a stirred tank may be a significant operating cost component. It can be produced by a reduction process involving a nickel solution and hydrogen gas. In a nickel reduction process, hydrogen gas must first dissolve into the bulk liquid and then adsorb onto the surface of the seed nickel particles before it can react with the ammoniacal nickel sulphate solution. The rate of the reaction, therefore, depends on the available nickel surface area[1]. The surface area available in turn depends on the amount of solids suspended. Axial impellers have traditionally been employed to provide a suspension of solids[2,3]. In solids suspension, the first step is to achieve just off-bottom suspension and subsequently increase the axial and radial distribution of the solids. Much work has been done on determining the impeller speed required to achieve just suspended solids as described by Zweitering[4]. The axial impellers, which include the pitched blade impellers, marine propeller and hydrofoil propeller, generate high circulation flows resulting in a relatively uniform solids concentration distribution. Barresi and Baldi[5] employed sampling methods to determine solids concentration distribution, and Montante *et al.*[6] studied the same mixing feature using computational fluid dynamics (CFD) techniques. Many studies on the concentration distribution have focused on solids with relatively low density and low loading, such as glass and sand[7–9]. Barrue *et al.*[9] employed the black box impeller modelling approach (IBC) to study solids suspension in a high solids volume fraction (20 per cent) system. However, it has been reported that results obtained with the black box approach have limited application to other systems[10].

* *Department of Chemical Engeering, Vaal University of Technology, Vanderbijlpark, South Africa.*

† *Department of Chemical and Metallurgical Engineering, Tshwane University of Technology, Pretoria, South Africa.*

‡ *Department of Chemical and Process Engineering, Moi University, Kenya*

 SA ISSN 0038–223X/3.00 + 0.00. Paper received Feb. 2009; revised paper received Nov. 2009.

CFD simulation and experimental measurement of nickel

The simulation of high solids loading systems has been limited by the type of drag curves used in most commercial software. However, it has been shown[11] that the Gidaspow drag curve[12] gives results of solids concentration distribution for high solids loading (10–20 per cent) that compare well with experimental data even for high density (8 900 kgm^{-3}) particles. One of the experimental methods that has been used very successfully to determine the solids concentration distribution is the optical attenuation technique (OAT), which was developed by Fajner *et al.*[13].

In the present work, solids concentration distribution of high density solids has been investigated using the OAT and CFD techniques with the Gidaspow drag curve[12] and the results obtained with nickel particles have been compared with those obtained with glass and sand particles.

Experimental and simulation techniques

The fluid flow pattern and solids suspension studies were carried out in a dish-bottomed tank stirred by a hydrofoil propeller using both experimental and CFD methods. The experimental methods were employed to obtain detailed information on the flow field as well as the solids concentration distribution, and these were compared with the simulation results. The simulations were run using the CFX code[14] for both liquid-only and solid-liquid systems. Solids loading was based on volume fraction (v/v_o), where v is the volume of the particles and v_o is the volume of liquid-solid mixture.

Experimental techniques

The flow field for the mean velocity was measured by the laser Doppler velocimetry technique (LDV) as described by Ochieng *et al.*[15]. The LDV results were used to validate the flow field predictions obtained by the CFD technique. Solids concentration was determined by both an optical attenuation technique (OAT), originally proposed by Fajner *et al.*[13] and by a sampling method. The optical method employed in the present work was adopted from that developed by Fajner *et al.*[13] with provision for determining the fine particle settling velocity.

LDV measurements

The LDV measurements were taken for the three-dimensional mean velocity and turbulent fields in a Perspex vessel, which provided a good refractive matching between the tank and water for the measurement. The LDV probe was mounted on a robotic arm and the measurements of the three velocity components were taken in the middle of two baffles ($\theta = 0^o$).

Optical attenuation technique (OAT)

The non-intrusive optical attenuation technique works on the principle that the attenuation of light passing through slurry depends on the solids concentration on the light path. Light was transmitted from an infrared light emitting diode (LED) through the tank to a photodiode (PD) on the opposite side of the tank, as shown in Figure 1. The output signal from the receiver was processed by an integrated circuit (IC) unit.

There is a linear relationship between the light intensity received and the output voltage, and therefore, the output voltage was taken as a measure of the light intensity. The output of the PD was then passed through a combination of amplification and filtering in the IC. There was also a synchronous detection system incorporated, which sampled the signal only at the precise time of transmission. Sampling was done at a rate of 100 per second. During the inactive transmission period, the output of the receiving device was inverted. What followed was a direct current (DC) component of the signal.

A low pass filter cleaned up the DC component, which was then fed into an operational amplifier set-up in voltage following mode. This drives the signal with high impedance. This analogue signal was digitally converted at a chosen frequency using a data acquisition board and stored in a PC. The light intensity indicated by the signals from the IC was a measure of the quantity of particles suspended on the light path. Three samples were taken at a given point and the average of these represented the solids concentration on the horizontal plane at the point of measurement. Measurements were taken above the curved bottom region of the tank up to a point 2 cm from the surface of the liquid at rest. There was a total of 28 axial data sampling points corresponding to an interval length of two cells in the CFD model of the structured grid.

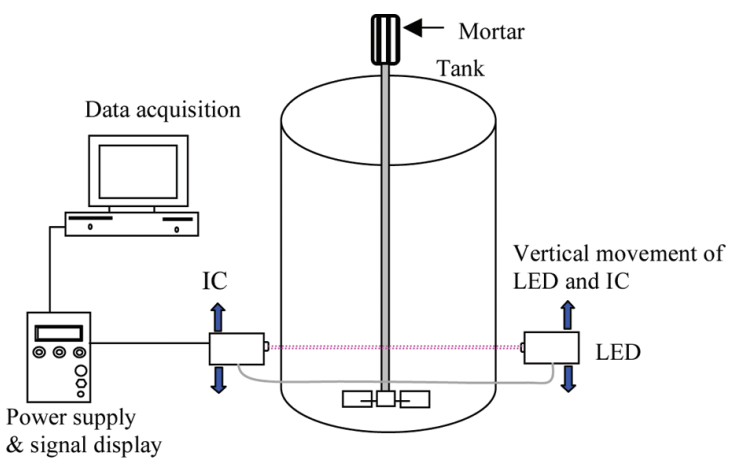

Figure 1—Schematic diagram of the optical attenuation experimental set-up

The system was calibrated with different particle sizes, and the relation between the output voltage from the IC and the solids concentration followed a logarithmic function, as shown in Figure 2. The output signal (I) was normalized with respect to the signal obtained in the particle free liquid (Io). The intensity of signals passing through the tank for a given solids mass increased with particle size. This is due to the fact that the smaller particles have a larger surface area to mass ratio; therefore, for a given solid mass, the small particles obstruct more light than the bigger ones.

Solids concentrations up to 500 g (1.33 per cent) loading of Ni particles with a diameter of 230 m could be measured within a standard deviation error acceptable in this study (about 8 per cent). A higher loading resulted in a rapid increase in the measurement error up to 70 per cent for a 1 kg loading; therefore, the maximum loading was taken as 1.33 per cent. The correlation for the solids concentration is a Lambert-Beer-type of equation[16], which holds for intensity attenuation of a narrow beam of light traversing dilute particle dispersions. The solids concentration (c) is calculated as:

$$c = a_o \ln\left(\frac{I}{I_o}\right) \quad [1]$$

where a_o is the constant that depends on the path length and particle size, I/I_o is the normalized output signal. In this application, the path length was constant.

Sampling method

Isokinetic sampling is known to improve the accuracy of the sampling method. However, to avoid settling of the particle in the sampling tube, the sampling velocity was set to 3 times the mean particle settling velocity. The sampling tube diameter was 15 times the diameter of the largest particles. On the one hand, a small sampling tube diameter would result in an increase in the wall effect, and on the other hand, a large diameter would result in a low sampling velocity or a high sampling volume. Since the ratio of the tank diameter to that of the particles (d_{50}) was 1 500, the wall effect was neglected in computing the particle settling velocity. Samples were taken from 7 radial and 16 axial points. Each radial location represented a set of axial points, one of which was 20 mm from the tank wall[5]. Three samples were taken from each point, out of which the mean value was obtained.

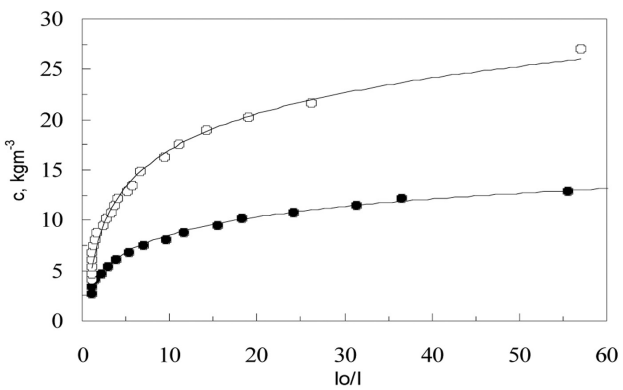

Figure 2—Variation of solids concentration (c) with output signal (I/Io): (o) Ni230, (•) Ni400, (—) Logarithmic fit

Simulation techniques

The Reynolds Averaged Navier-Stokes (RANS) equations are expressed in terms of the mean quantities and the terms arising from the averaging procedure. For multiphase systems, the RANS equations are modified with the introduction of phase hold-up and interfacial related forces. The solid-liquid system was modelled using the Eulerian two-fluid method. A free surface boundary condition was defined at the liquid surface, where the shear stresses were set to zero. The blades, disc (for the Rushton turbine) and baffles were defined as thin surfaces, and grids were refined in the wall and impeller regions. On the walls, a no-slip condition was specified for the liquid, while free slip was specified for the particles. Initial and final simulation runs were done using the multiple frame of reference (MFR) and sliding grid (SG) impeller simulation approaches respectively. In the SG approach, the inner block rotates while the outer one is stationary, and for both MFR and SG, the radial location of the interface with respect to tank diameter (T) was at 0.585 T. The bottom part of the rotating block was set to rotate in the opposite direction, making it stationary with respect to the stationary frame. The interconnectivity between the rotating and stationary domain was achieved by the general grid interface (GGI) algorithm[14].

Governing equations

The governing equations are given in a time averaged form, in which conservation of mass is:

$$\frac{\partial}{\partial t}\left(\rho_n \varphi_n\right) + \nabla \cdot \left(\rho_n \varphi_n \boldsymbol{U}_n - \nabla D_{LS} \varphi_n\right) = 0 \quad [2]$$

where φ_n is the phase hold-up for phase 'n', ρ and $\boldsymbol{U}$ are the density and the mean velocity vector, respectively and D_{LS} is the turbulent diffusivity, which is specified if the Reynolds averaging approach is used, otherwise it is set to zero for the Favre-averaged equations. The momentum conservation equation for the liquid phase is given by:

$$\frac{\partial}{\partial t}\left(\rho_L \varphi_L \boldsymbol{U}_L\right) + \nabla \cdot \left(\rho_L \varphi_L \boldsymbol{U}_L \otimes \boldsymbol{U}_L\right) = -\varphi_L \nabla \cdot p + F_I + F_B + \varphi_L \nabla \cdot \boldsymbol{\tau}_L \quad [3]$$

where F_B represents body forces including gravity, Coriolis and centrifugal force; p is the pressure and F_I represents the interfacial forces, of which drag is the most important. The momentum balance for the solid phase has an additional term that accounts for the interaction between the particles, and is given by:

$$\frac{\partial}{\partial t}\left(\rho_s \varphi_s \boldsymbol{U}_s\right) + \nabla \cdot \left(\rho_s \varphi_s \boldsymbol{U}_s \otimes \boldsymbol{U}_s\right) = -\varphi_s \nabla \cdot p - \nabla \cdot p_s + \varphi_s \nabla \cdot \boldsymbol{\tau}_s + \varphi_s \nabla \cdot \boldsymbol{\tau}_L + F_I + F_B \quad [4]$$

where p_s is the solid pressure[12] that accounts for interaction between the particles, τ_s is the solids stress, which was neglected in the present study.

Implementation of the modelling equations

The k-ε turbulence model was employed with both the multiple frame of reference (MFR) and sliding grid (SG) approaches. Initial flow fields were obtained with the MFR approach whereas the final results were obtained with the SG approach for both single and multiphase simulations. Three

grid sizes were used to model a quarter of the tank with one impeller blade: 109 000; 263 000 and 350 000 cells. The solids loading was up to 10 per cent, for 230 m diameter particles of sand, glass and nickel (Ni).

Results and discussion

The CFD prediction of the nickel solids concentration distribution was compared with experimental results obtained with both the sampling and optical attenuation methods, and it was shown that there was a reasonable comparison between results obtained with the optical attenuation and simulation methods. The nickel solids concentration distribution differed significantly from those of glass and sand due to its high density compared to that of the other two particles.

Comparison between the sampling and optical methods

In Figure 3, the results for the normalized solids volume fraction obtained by the wall sampling method deviated from unity by as much as 50 per cent. Even with the method of the mean of samples, the axial solids distribution was still high (up to 25 per cent deviation from unity) in comparison to both the CFD and OAT methods. The apparent accumulation of the solids in the wall region is an indication that taking samples in this region, as has been a common practice[5], is a misrepresentation of the solids concentration in a tank.

Effect of solids loading on the axial velocity

It is shown in Figure 4 that a good comparison was obtained between the experimental and the simulation results of the axial velocity for a zero solid loading system. The introduction of the solids into the system resulted in a decrease in the axial velocity by up to 50 per cent in the wall region. This can be attributed to the accumulation of the solids in the wall region as shown by the wall sampling method in Figure 3. The interaction between impeller tip generated stream and the tank bottom wall results in a wall jet[17]. This wall jet is responsible for the upward axial velocity. In a case where solids tend to accumulate in the wall region, the wall jet was attenuated by the solids and hence the axial velocity component.

Radial solids concentration distribution

At the impeller N_{js} speed of 674 rpm, it is shown in Figure 5 that the nickel solids concentration gradient varied in the radial directions. This observation is different from the uniform radial solids distribution that was reported for sand and glass particles[5,6] in a system stirred by multiple impellers. In the present case, unlike that reported by these authors, the tank was stirred by only one impeller. Moreover, due to the high density, the nickel particles tend to settle more rapidly than sand and glass in regions away from the impeller. Tanks stirred by single impellers are the most common configurations in practical applications, and the present results show that in such systems, there is a relatively low concentration of solids in the middle of the tank. The results indicate that nickel solids suspension and distribution can be improved by multiple impellers and results reported elsewhere[15,18] indicate that the bottom impeller could be a Rushton turbine located closer to the tank bottom.

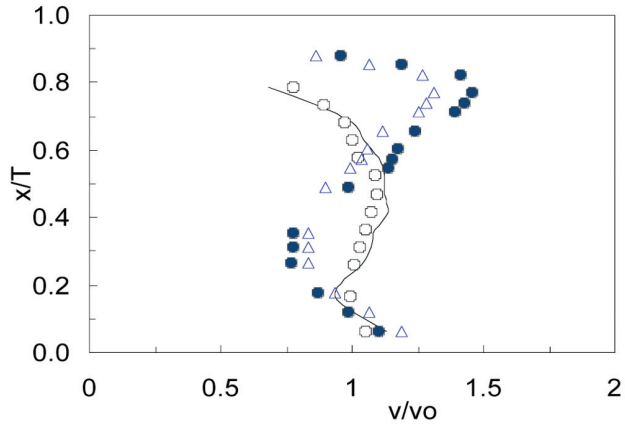

Figure 3—Variation of dimensionless solids volume fraction (v/vo) with normalized tank height (x/T) for 1.33% Ni at 420 rpm: (o) OAT, (—) CFD, (•) Sampling at 22 mm from the wall, (Δ) mean of radial points

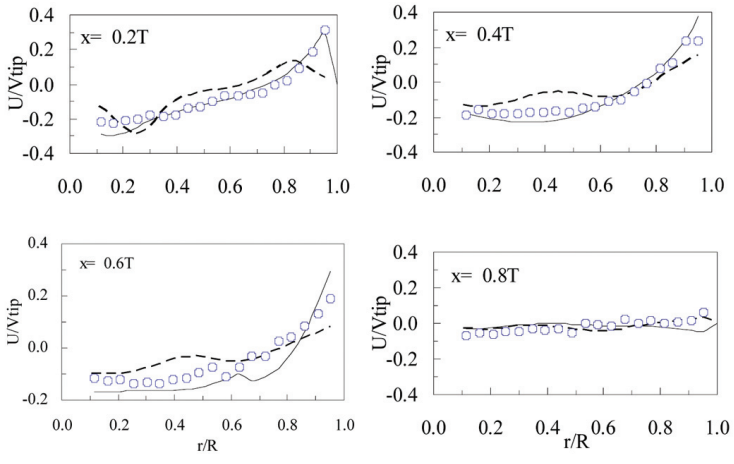

Figure 4—Effect of Ni solids loading on the axial velocity at 420 rpm: (o) LDV–0% (—) CFD-0%; (Δ) CFC–1.33%

CFD simulation and experimental measurement of nickel

Particle density effect

The density of nickel particles is very high (8 903 kg/m^3) compared to that of water, and the requirement that a complete suspension be achieved in order to maximize the surface area available for crystal growth, poses a great challenge. Table I shows experimentally determine terminal settling velocity (U_T) and other hydrodynamic parameters for the three different particle types. The maximum Stokes number (St), which is the ratio of the Stokesian particle relaxation time to the time required for one impeller revolution, was 0.76. The difference between the Archimedes number (Ar) for nickel and sand of the same size was more than one order of magnitude. A high Ar is indicative of the importance of the free stream turbulence on solids suspension. A comparison between the concentration profiles for these particles is presented in Figure 6, where the nickel concentration profile is shown to deviate from the profile of the other particles. The relative difference in the concentration profile of sand and glass was about 6 per cent whereas that for the nickel deviated from the two others by up to 20 per cent in most regions in the tank. Again, particles with higher densities accumulated more in the bottom region than the low density ones.

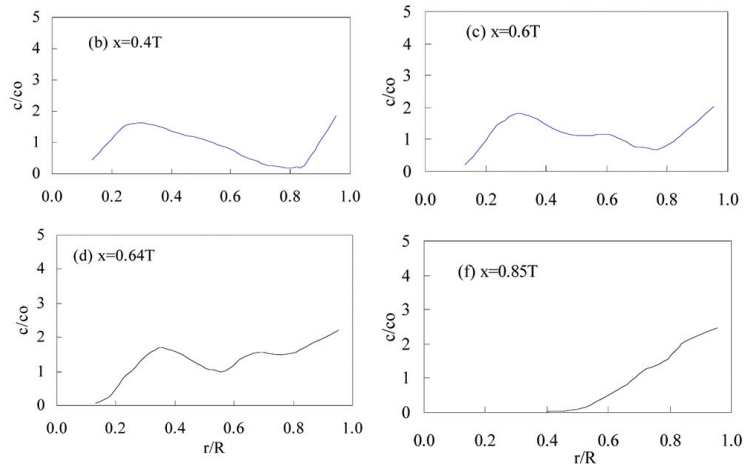

Figure 5—Variation of solids concentration with the radial distance (r/R), 10% Ni loaging, 674 rpm

Table I

Hydrodynamic properties for nickel, sand, and flint glass

Particle	d_p, micron	Density, kgm^{-3}	Terminal settling velocity U_T, m^{-1}	Reynolds no. R_{ep}	Froud no. Fr	Stokes's no. St	Archimedes no. Ar
Nickel	75–1000	8903	0.037–0.35	2.36–271.7	0.67–1.89	0.0025–0.76	41–97643
Flint glass	750	4200	0.182	136	0.746	0.268	16689
Sand	750	2500	0.111	83.5	0.378	0.191	7831

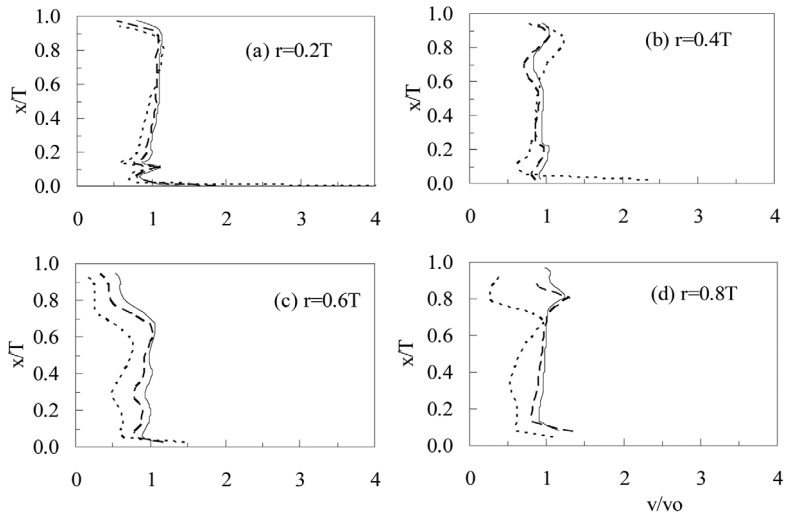

Figure 6—Variation of volume fraction with particle density, 10% loading at 500 rpm: (—) sand, (– – –) glass, (– – – – – –) nickel

The region about the mid radial distance from the centre (the upper section of Figure 6 (b-d) is of special interest due to the fact that there was a higher concentration of nickel than sand and glass in this region, while it is expected that the nickel particles, being the most dense, would be the least suspended. It is important to note that this phenomenon is similar to what has been observed with the larger particles[18]. This (as is in the case of the larger particles) can again be attributed to the higher inertial force that the nickel particles have, in comparison to the sand and glass particles. In this region, the liquid current caused by the wall jet suddenly changes direction, from upward flow to downward flow. The particles with a higher inertial force are expected to continue with the initial trajectory long after the liquid and smaller particles have changed course to downwards motion. The change of direction for the larger or heavier particles is eventually expected to take place in the region closer to the centre of the tank than in the case of the lighter or smaller particles. Therefore, this could lead to a higher concentration of the larger or heavier particles in this region. In a nickel batch precipitation process, the particle size increases with reaction time. In this context, these results indicate that nickel particle distribution and the subsequent power loading on the impeller would increase with an increase in time.

The axial concentration distribution increases with particle size and particle size distribution, and the influence of the turbulent dispersion force and solid pressure increase with an increase in the solids loading. It has been reported[18] that for low solids loading, the solids suspension is governed by the bulk fluid flow and the influence of non-drag forces, while the turbulent dispersion force is negligible. Such a system may be scaled up on the basis of the impeller tip speed[6]. However, for high solids loading, Montante and co-workers reported that turbulence intensity influences the solids suspension and that the scale-up may be based on power dissipated per unit volume. Scale-up of a system in which there exists the kind of inhomogeneity experienced with high density and heavy particles can be very challenging. For this reason, there is a need for further hydrodynamic investigation on the concentration distribution of high density solids and high solids loading. The solids loading employed in the present work was kept low due to the limitation of the computational power and the OAT equipment.

Conclusion

CFD simulation methods can be used, with drag curves that account for particle interaction, to predict the solids concentration distribution for a high solids loading (10–20 per cent) system. In this work the CFD simulation results were in better agreement with the experimental data obtained using the optical attenuation technique than those obtained using the sampling method. Solids concentration was shown to be highest both in the wall and impeller regions and these are the regions in which the axial velocity was highest. As a result of this, the wall sampling method overestimated the solids concentration. This shows that the conventional experimental method of determining solids concentration distribution through sampling does not accurately represent the overall solids concentration in the tank. The nickel solids gave a different concentration distribution pattern compared to those of the flint glass and sand particles. The results show the limitations of single impeller and indicate that nickel solids suspension and distribution could be improved using multiple impellers.

Acknowledgement

Contribution by Professor Alison A. Lewis is gratefully acknowledged. One of the authors (Ochieng) is grateful for the bursary received from Impala Platinum Ltd.

References

1. Willis, B. and Essen, J.V. Precipitation of nickel metal by hydrogen reduction: A new perspective*, Nickel, Cobalt Conference Proceedings*, Atlanta 2000 Nickel/Cobalt Conference, Perth, 15–17 May 2000.
2. Armenate, P.M. and Nagamine, E.U. Effect of low off-bottom impeller clearance on the minimum agitation speed for complete suspension of solids in stirred tanks, *Chemical Engineering Science,* vol. 53, no. 9, 1998. pp. 1757–1775.
3. Kuzmanic, B. and Ljubicic, N. Suspension of floating solids with up-pumping pitched blade impellers; mixing time, power characteristics, *Chemical Engineering Journal*, vol. 84, no. 3, 2001. pp. 325–333.
4. Zwietering, T.N.H. Suspending of solids particle in liquid by agitators, *Chemical Engineering Science*, vol. 8, 1958. pp. 244–253.
5. Barresi, A. and Baldi, G. Solids suspension in an agitated vessel, *Chemical Engineering Science*, vol. 42, no. 12, 1987. pp. 2949–2956.
6. Montante, G., Pinelli, D., and Magelli, F. Scale up criteria for the solids distribution in a slurry reactor stirred with multiple impellers, *Chemical Engineering Science*, vol. 58, 2003. pp. 5363–5372.
7. Mersmann, A., Werner, F., Maurer, S., and Bartosch, K. Theoretical prediction of the minimum stirrer speed in mechanically agitated suspensions, *Chemical Engineering and Processing*, vol. 37, no. 6, 1998. pp. 503–510.
8. Kee, C.S. and Tan, B.H.R. CFD simulation of solids suspension in mixing vessels, *The Canadian Journal of Chemical Engineering*, vol. 80, 2002. pp. 1–6.
9. Barrué, H., Karoui, A. N. Le Sauze, J. and Costes, F. Illy, Comparison of aerodynamics and mixing mechanisms of three mixers: Oxynator™ gas–gas mixer, KMA and SMI static mixers, *Chemical Engineering Journal*, vol. 84, no. 3, 2001. pp. 343–354.
10. Brucato, A. Ciofalo, M., Grisafi, F., and Micale, G. Numerical prediction of flow fields in baffled stirred vessels: A comparison of alternative modelling approaches, *Chemical Engineering Science*, 1998b, vol. 53, no. 21. pp. 3653–368.
11. Ochieng, A. and Onyango, M.S. Drag models and solids concentration distribution in a stirred tank, *Powder Technology*, vol. 181, 2008. pp. 1–8.
12. Gidaspow, D. Multiphase flow, fluidization: Continuum, kinematic theory description, *Academic Press*, New York. 1994.
13. Fajner, D., Magelli, F., Nocentini, M., and Pasquali, G. Solids concentration profiles in a mechanically stirred, staged column slurry reactor, *Chemical Engineering Research and Design*, vol. 63, 1985. p. 235.
14. AEA Technology. CFX5 Flow solver user guide, Computational Fluid Dynamics Services, Harwell, Oxfordshire UK: AEA Industrial Technology. 2003.
15. Ochieng, A., Onyango, M.S., Kumar, A., Kiriamiti, H.K., and Musonge, P. Mixing and power draw in a tank stirred by a Rushton turbine at a low clearance, *Chemical Engineering and Processing Journal*, vol. 47, no. 5, 2008. pp. 842–851.
16. Brucato, A., Grisafi, F., and Montante, G. Particle drag coefficients in turbulent fluids. *Chemical Engineering Science*, vol. 53, no. 18, 1998a. pp. 3295–3314.
17. Bhattacharya, S. and Kresta, S.M. CFD simulations of three-dimensional wall jets in a stirred tank, *Canadian Journal of Chemical Engineering*, vol. 80, no. 4, 2002. pp. 695–709.
18. Ochieng, A., Alison, E. Lewis. CFD simulation of nickel solids concentration distribution in a stirred tank. *Minerals Engineering Journal*, vol. 19, 2006. pp. 180–189. ◆